

Uncertainty-Aware Unsupervised Image Deblurring with Deep Priors Guided by Domain Knowledge

Xiaole Tang¹ Xile Zhao^{1*} Jun Liu² Jianli Wang¹ Yuchun Miao¹ Tieyong Zeng³

¹University of Electronic Science and Technology of China, Chengdu, China

²Northeast Normal University, Shenyang, China

³The Chinese University of Hong Kong, Shatin, NT, Hong Kong

{sherlock315, xlzhao122003, junliu2, wangjianli123, szmyc1}@163.com, zeng@math.cuhk.edu.hk

Abstract

Non-blind deblurring methods achieve decent performance under the accurate blur kernel assumption. Since the kernel error is inevitable in practice, ringing artifacts are often introduced by non-blind deblurring. Recently, semi-blind deblurring methods can handle kernel uncertainty by introducing the prior of the kernel (or induced) error. However, how to design a suitable prior of the kernel (or induced) error remains challenging. Hand-crafted prior, incorporating domain knowledge, generally performs well but may lead to poor performance when kernel (or induced) error is complex. Data-driven prior, which excessively depends on the diversity and abundance of training data, is vulnerable to out-of-distribution blurs and images. To address this challenge, we suggest a data-free deep prior for the kernel induced error (termed as residual) expressed by a customized untrained deep neural network, which allows us to flexibly adapt to different blurs and images in real scenarios. By organically integrating the respective strengths of deep priors and hand-crafted priors, we propose an unsupervised semi-blind deblurring model which recovers the latent image from the blurry image and inaccurate blur kernel. To tackle the formulated model, an efficient alternating minimization algorithm is developed. Extensive experiments demonstrate the superiority of the proposed method to both data-driven prior and hand-crafted prior based methods in terms of the image quality and the robustness to the kernel error.

1. Introduction

Image blurring is mainly caused by camera shake [23], object motion [7] or defocus [35]. By assuming the blur kernel is shift-invariant, the image blurring can be formulated as the following convolution process:

$$\mathbf{y} = \mathbf{k} \otimes \mathbf{x} + \mathbf{n}, \quad (1)$$

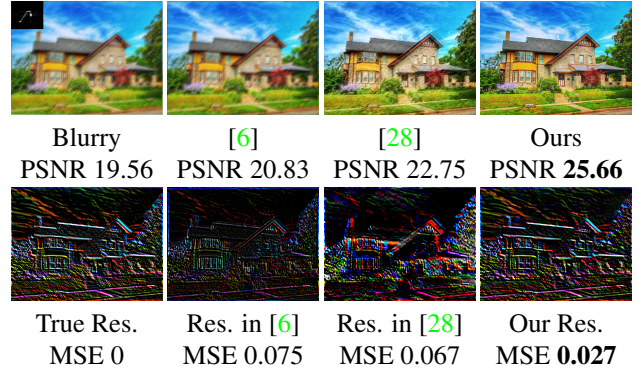


Figure 1. Visual comparison of the restored results of three semi-blind methods based on different priors for the residual induced by the kernel error, including hand-crafted prior [6], data-driven prior [28], and the proposed deep residual prior (DRP) guided by the domain knowledge (i.e., the sparse prior). The first row contains the blurry image and restored images while the second row contains the true and estimated residuals. The true residual is a convolution of the kernel error and the clean image (i.e., $\mathbf{r} = \Delta \mathbf{k} \otimes \mathbf{x}$).

where \mathbf{y} , \mathbf{x} denote the blurry image and clean image respectively, \mathbf{k} represents the blur kernel, \mathbf{n} represents the additive Gaussian noise, and \otimes is the 2D convolution operator.

Image deblurring has received considerable research attention. In terms of the availability of kernel, current image deblurring methods can be mainly classified into: 1) *blind deblurring methods* in which the blur kernel is assumed to be unknown; 2) *non-blind deblurring methods* in which the blur kernel is assumed to be known or computed elsewhere. A typical blind deblurring method generally involves two stages: estimating the blur kernel from the blurry images, and then recovering the latent image with the estimated blur kernel. For the kernel estimation, a plethora of prior knowledge is introduced to model blur kernels [8, 12, 15, 17, 22, 25, 26, 31, 36]. With the known blur kernel, a variety of non-blind deblurring approaches,

based on total-variation [29], hyper-Laplacian [10], nonlocally centralized sparse representation [3], and deep learning [32, 33], are suggested to recover the latent image from the blurry image.

Most existing non-blind deblurring methods are developed to perform well under the error-free kernel assumption. However, in the real application of non-blind methods, the kernel estimation is hardly accurate owing to the ill-posedness of such an inverse problem. As a result, these methods without handling kernel uncertainty often lead to unpleasant performance such as introducing ringing artifacts. This implies the significance of semi-blind deblurring methods that take measures to handle kernel uncertainty.

Recently, semi-blind deblurring methods handle kernel uncertainty by introducing the prior for the kernel (or induced) error. However, how to design a suitable prior of the kernel (or induced) error remains challenging. In the literature, there are two groups of priors of kernel (or induced) error, i.e., hand-crafted and data-driven priors. Hand-crafted priors [6, 34], incorporating domain knowledge, generally perform well but may lead to poor performance when the distribution of kernel (or induced) error is complex due to its insufficient representation ability. For example, such hand-crafted priors are insufficient for the characterization of complex intrinsic structure (see Figure 1) of the kernel induced error (termed as residual). Data-driven priors [16, 21, 28], which excessively depend on the diversity and abundance of training data, are vulnerable to out-of-distribution blurs and images (see Figure 1). Therefore, it is highly desired to design a new prior for the kernel (or induced) error that can overcome the issue of data starvation while maintaining fine representation ability.

To address this challenge, we suggest a data-free deep prior called deep residual prior (DRP) for the residual, which leverages the strong representation ability and unsupervised nature of unsupervised neural networks. Specifically, DRP is expressed by a customized untrained deep neural network, where a soft-shrinkage based block is embedded in the downsampling and upsampling layers. Moreover, by leveraging the advantage of hand-crafted prior that exploits the domain knowledge, we use the sparse prior to guide DRP to form a semi-blind deblurring model. This model organically integrates the respective strengths of deep priors and hand-crafted priors to achieve better performance. To the best of our knowledge, it is the first attempt to handle kernel uncertainty for image deblurring in an unsupervised manner.

In summary, Our contributions are mainly three-fold:

- We propose a tailored DRP guided by the general domain knowledge for the residual induced by the kernel error. This integration allows us to better characterize the complex structure of the residual compared to the existing priors, including hand-crafted priors and data-driven priors.

- We propose a semi-blind deblurring model which organically integrates the respective strengths of deep priors and hand-crafted priors. An alternating minimization algorithm is proposed to solve the corresponding optimization problem.

- Extensive experiments with multiple scenarios show the effectiveness, adaptability to different blurs and images, and the robustness to the kernel error of the proposed method; see Figure 1 for a toy example.

2. Related Works

In this section, we give a detailed introduction about the semi-blind deblurring methods that focus on handling the kernel error.

Model-based methods are dominating in the early literature of semi-blind deblurring. These methods generally handle the kernel error with some hand-crafted priors. For example, Zhao *et al.* [34] directly treated the kernel error as additive zero-mean Gaussian white noise (AGWN), and l_2 -regularization is utilized to model it. Ji & Wang [6] treated the residual as an additional variable for estimation, which is done by regularizing it via a sparse constraint in the spatial domain (i.e., l_1 -related regularization). However, such hand-crafted priors are highly dependent on certain statistical distribution assumptions, such as sparsity and AGWN assumptions, which do not always hold true in practice. Thus, such methods are efficient sometimes but not flexible enough to handle the kernel error in complex real scenarios.

Recently, triggered by the expressing power of deep neural networks, many deep learning-based methods have emerged, in which data-driven priors are learned from a large number of external data for handling kernel error. For such methods, the key factor to success is how to design an appropriate neural network structure. For instance, Ren *et al.* [20] proposed a partial convolution model with the estimation of a confidence map for modeling kernel estimation error in the Fourier domain. Vasu *et al.* [28] trained their CNNs with a large number of real and synthetic noisy blur kernels to achieve good performance for image deblurring with inaccurate kernels. Ren *et al.* [21] proposed a general maximum a posterior (MAP) based framework to tackle the image restoration task with an inaccurate degradation model. Nan and Ji [16] unrolled an iterative total-least-squares estimator in which the kernel error-related prior (i.e., residual prior) are learned by their customized supervised Dual-path U-Net. Although these data-driven kernel error priors are attractive when pursuing high-quality recovered images, the limitation is also widely recognized. They excessively depend on the diversity and abundance of training data and are vulnerable to out-of-distribution blurs and images.

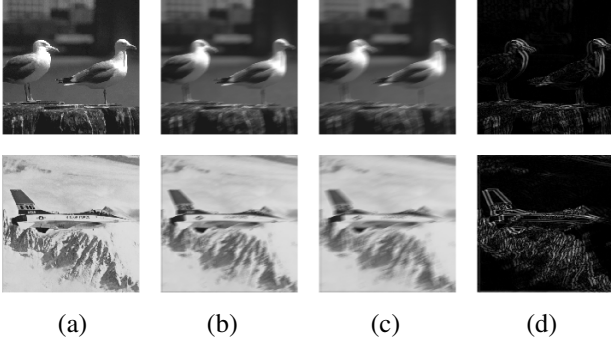


Figure 2. Visualization of the residual with inaccurate kernels. (a)-(d): Clean images; Blurry images with the true kernel (motion blur with length of 20 pixels and orientation of 10°); Blurry images with the inaccurate kernel (motion blur with length of 20 pixels and orientation of 20°); The residuals induced by the kernel error.

3. Proposed Method

In this paper, we propose a data-free deep prior for the residual induced by the kernel error expressed by a customized untrained deep neural network, which allows us to flexibly adapt to different blurs and images in real scenarios. By organically integrating the respective strengths of deep priors and hand-crafted priors, we propose an unsupervised semi-blind deblurring model which recovers the latent image from the blurry image and inaccurate blur kernel.

3.1. Problem Formulation

To this end, we first take a look at the formulation of the semi-blind deblurring problem. In the presence of the kernel error, the degradation process (1) can be rewritten as

$$\mathbf{y} = (\hat{\mathbf{k}} + \Delta\mathbf{k}) \otimes \mathbf{x} + \mathbf{n} = \hat{\mathbf{k}} \otimes \mathbf{x} + \underbrace{\Delta\mathbf{k} \otimes \mathbf{x}}_{\mathbf{r}} + \mathbf{n}, \quad (2)$$

where \mathbf{y} , \mathbf{x} denote the blurry image and clean image respectively, \mathbf{k} represents the blur kernel, \mathbf{n} represents the AGWN, \otimes is the 2D convolution operator, and $\mathbf{r} = \Delta\mathbf{k} \otimes \mathbf{x}$ is the residual induced by the kernel error.

To suppress the ringing artifacts resulting from inaccurate kernel, we consider involving ringing artifact \mathbf{h} in (2):

$$\mathbf{y} = \hat{\mathbf{k}} \otimes \mathbf{x} + \mathbf{r} + \mathbf{h} + \mathbf{n}. \quad (3)$$

3.2. Optimization Model

Note that deriving \mathbf{x} , \mathbf{h} , \mathbf{r} from the blurry image \mathbf{y} is a typical ill-posed problem which admits infinite solutions. To overcome such ambiguity and confine the solution space, prior information of \mathbf{x} , \mathbf{h} , \mathbf{r} is required. In this work, the proposed DRP incorporated with the sparse prior for the residual \mathbf{r} , DIP incorporated with total variation for the latent image \mathbf{x} , and the sparse prior in the DCT domain for the artifact \mathbf{h} are utilized. The motivations are as follows.

Deep Residual Prior and the Sparse Prior for \mathbf{r} . Since the residual induced by the kernel error, containing high-frequency components images, is not a common natural image (see Figure 2), we utilize the DRP guided by the sparse prior to model the residual \mathbf{r} induced by the kernel error.

Due to the complex blurring process, it is challenging to model the residual \mathbf{r} accurately by hand-crafted priors or data-driven priors. In fact, we demand to flexibly model the residual \mathbf{r} of a practical blurring process that might be extremely complex. Thus, an unsupervised network becomes a natural choice, which possess both strong representation ability and adaptability to different data. Here, we employ a tailored unsupervised network structure—the customized U-Net architecture (see Figure 5) to capture the residual \mathbf{r} , which encourages the sampling of the prior information of the residual \mathbf{r} . Furthermore, since deep priors are sampled from degraded signals, simply using deep priors will lead to unwanted local minimizers and even degraded results. In the meantime, high-frequency signals are contained in the residual \mathbf{r} . To overcome these two issues and confine the solution space, the sparse prior is utilized as the domain knowledge to guide DRP. These two priors are organically combined to more accurately model the residual \mathbf{r} .

Deep Image Prior and Total Variation for \mathbf{x} . Recently, DIP has shown promising performance in various image restoration tasks [5, 19, 27]. For modeling the latent image \mathbf{x} , we utilize the DIP and total variation to depict the complex structures of the image and its local smoothness, whose effectiveness is verified in the work [19].

Sparse Prior in the DCT Domain for \mathbf{h} . It is worth noting that ring artifacts \mathbf{h} caused by the kernel error $\Delta\mathbf{k}$ generally have strong periodicity around the sharp edges. Since the DCT coefficient vector $\mathbf{v} = \mathcal{C}\mathbf{h}$ is sparse [6], where \mathcal{C} is the DCT operator, it is reasonable to impose sparse prior on ringing artifacts \mathbf{h} in the DCT domain.

Following the above argument, we propose a semi-blind deblurring model. The overview of our model is illustrated in Figure 3. In the overall model, the proposed DRP is combined with the sparse prior for the residual \mathbf{r} and DIP is combined with total variation for the latent image \mathbf{x} . Along with the sparse prior in the DCT domain for ringing artifacts \mathbf{h} , these priors can be organically integrated to form an unsupervised loss, in which all priors interact with each other to more accurately estimate the components in the degradation process. The minimization model is formulated as follows:

$$\min_{\theta, \zeta, \mathbf{v}} \mathcal{D}(\theta, \zeta, \mathbf{v}) + \lambda_1 \|\mathcal{I}_\theta(\mathbf{z}_x)\|_{\text{TV}} + \lambda_2 \|\mathcal{R}_\zeta(\mathbf{z}_r)\|_1 + \lambda_3 \|\mathbf{v}\|_1, \quad (4)$$

with

$$\mathcal{D}(\theta, \zeta, \mathbf{v}) = \left\| \mathbf{y} - \hat{\mathbf{k}} \otimes \mathcal{I}_\theta(\mathbf{z}_x) - \mathcal{R}_\zeta(\mathbf{z}_r) - \mathcal{C}^T \mathbf{v} \right\|_F^2,$$

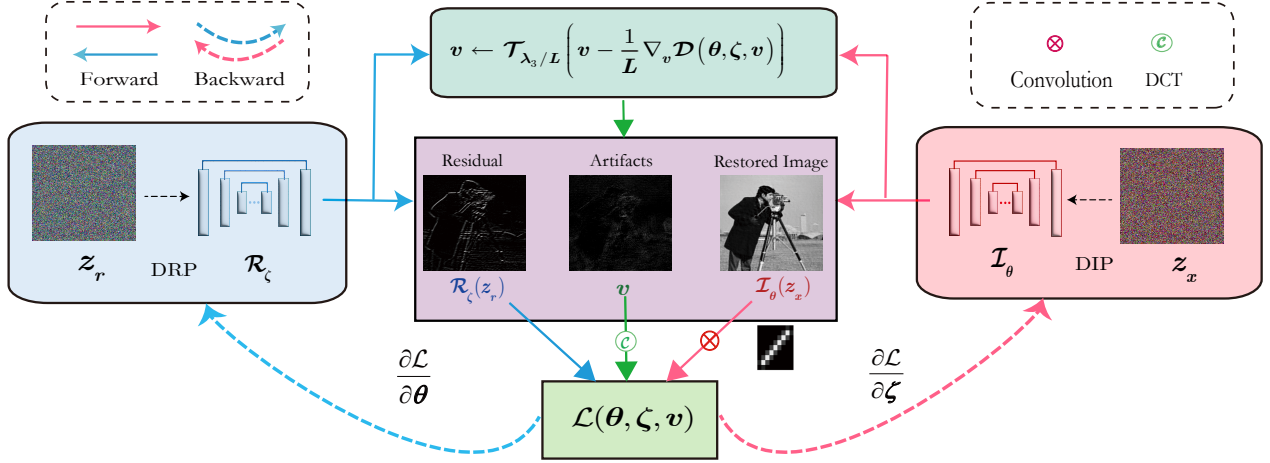


Figure 3. An overview of the proposed model. The DIP network estimates the restored image $\mathcal{I}_\theta(z_x)$ from random noise input z_x and the DRP network estimates the residual $\mathcal{R}_\theta(z_r)$ from random noise input z_r .

where $\mathcal{I}_\theta(\cdot) : \mathbb{R}^{n_1 \times n_2} \rightarrow \mathbb{R}^{n_1 \times n_2}$, and $\mathcal{R}_\zeta(\cdot) : \mathbb{R}^{n_1 \times n_2} \rightarrow \mathbb{R}^{n_1 \times n_2}$ are the neural networks used to capture the unsupervised DIP of the latent image x , and the proposed DRP of the residual r , respectively; θ and ζ collect the corresponding network parameters, respectively; z_x and z_r are random input of the neural networks responsible for generating the latent image x and residual r .

3.3. Optimization Algorithm

To simplify the representation, we denote the objective function in Eqn. (4) as $\mathcal{L}(\theta, \zeta, v)$.

Since the three variables are coupled, we propose to resolve the minimization problem (4) into two easier subproblems by the following alternating minimization scheme.

$$\{\theta^{i+1}, \zeta^{i+1}\} \in \arg \min_{\theta, \zeta} \mathcal{L}(\theta, \zeta, v^i), \quad (5)$$

$$v^{i+1} = \arg \min_v \mathcal{L}(\theta^{i+1}, \zeta^{i+1}, v), \quad (6)$$

where the superscript “ i ” is the iteration number.

$\{\theta, \zeta\}$ -subproblem: The subproblem (5) can be solved by using a gradient descent algorithm with adaptive momentum named Adam [9]:

$$\theta^{i+1} = \theta^i - \alpha_i \nabla_\theta \mathcal{L}(\theta, \zeta^i, v^i), \quad (7)$$

$$\zeta^{i+1} = \zeta^i - \alpha_i \nabla_\zeta \mathcal{L}(\theta^i, \zeta, v^i), \quad (8)$$

for all $i = 1, \dots, T$, where T is the preset maximum iteration number. Notably, the gradient w.r.t. θ^i, ζ^i can be computed by the standard back-propagation algorithm [24]. Here, α_i is an appropriate step-size (i.e., learning rate) of iteration number i , and it is determined by the step size rule advocated in the Adam algorithm [9].

v -subproblem: The subproblem (6) can be exactly solved using proximal gradient descent:

$$v^{i+1} = \mathcal{T}_{\lambda_3/L} \left(v^i - \frac{1}{L} \nabla_v \mathcal{D}(\theta^{i+1}, \zeta^{i+1}, v^i) \right), \quad (9)$$

where L is an adjustable constant, and \mathcal{T}_δ is the soft-threshold operator defined by

$$\mathcal{T}_\delta(a)_j = \max(|a_j| - \delta, 0) \operatorname{sgn}(a_j).$$

where a_j is the j th entry of vector a . The overall algorithm is summarized in Algorithm 1.

Algorithm 1 Numerical algorithm for solving (4)

Input: Blurry image y , inaccurate kernel \hat{k} , parameters L, λ_s ($s = 1, 2, 3$), and iteration number T .

Initialization: Random input $z_x \sim U(0, 1)$, $z_r \sim U(-0.5, 0.5)$.

- 1: **for** $i = 1$ to T **do**
- 2: $\hat{x}^{i+1} = \mathcal{I}_{\theta^i}(z_x), \hat{r}^{i+1} = \mathcal{R}_{\zeta^i}(z_r)$;
- 3: compute the gradient w.r.t θ and ζ ;
- 4: jointly update θ^i, ζ^i using Adam;
- 5: update v^{i+1} using (9);
- 6: **end for**

Output: the restored image \hat{x} and the residual \hat{r} .

4. Experiments

This section conducts extensive experiments to verify the adaptability to various blurs and images, the robustness to kernel error, and the effectiveness of the proposed method.

4.1. Experimental Setup

- **Model Hyperparameters Setting.** The model hyperparameters of the proposed method are $\{\lambda_i\}_{i=1}^3$ and

L . In all experiments, we empirically fix $L = 3$. Then $\{\lambda_i\}_{i=1}^3$ are tuned to obtain the best PSNR value. To investigate the influences of different model hyperparameters, we conduct experiments (see supplementary materials) on the simulated data. Based on the best PSNR/SSIM values, λ_1 , λ_2 , λ_3 are finally determined to be 5×10^{-2} , 5×10^{-5} , 5×10^{-7} , respectively.

- **Algorithm Hyperparameters Setting.** In all experiments, we set the total iteration number of the proposed algorithm to be 1500. The default learning rates of networks \mathcal{I}_θ and \mathcal{R}_ζ are respectively 9×10^{-3} and 5×10^{-4} .
- **Platform.** In this work, all experiments are conducted on the PyTorch 1.10.1 and MATLAB 2017b platform with an i5-12400f CPU, and RTX 3060 GPU, and 16GB RAM.

4.2. Ablation Study

The ablation studies primarily focus on two aspects: *a*) exploring the influence of DRP and the hand-crafted priors in our model; *b*) exploring the superiority of the tailored DRP architecture compared to other classical deep prior structures in fitting the residual induced by kernel error.

4.2.1 The Influence of DRP and Hand-crafted Priors

We evaluate the influence of hand-crafted priors that guide deep priors in our model on the testing images in Figure 4.



Figure 4. Sharp images used for specialized blur dataset.

Table 1. The average quantitative results produced by reconciling different hand-crafted priors with deep priors.

Method	PSNR	SSIM
w/o sparse prior for \mathbf{r}	26.52	0.844
w/o sparse prior for \mathbf{v}	25.98	0.832
w/o total variation for \mathbf{x}	27.87	0.868
w/o DRP for \mathbf{r}	25.33	0.821
Ours	28.48	0.887

Table 1 displays the average quantitative results produced by reconciling different hand-crafted priors with deep priors. It shows that the total variation imposed on latent image \mathbf{x} brings around 0.6 dB performance gain for the PSNR

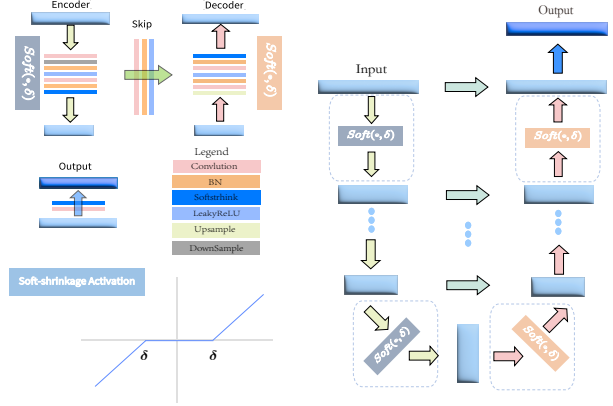


Figure 5. The illustration of the DRP network architecture—the customized U-Net, which learns a mapping from the random noise input \mathbf{z}_r to the residual \mathbf{r} .

index. The sparse prior for \mathbf{r} boosts the PSNR with around 2.0 dB performance gain. The sparse prior for \mathbf{v} brings about 2.5 dB performance gain. By the way, DRP, as the core prior modeling the residual, brings around 3.2 dB performance gain. This supports our analysis that deep priors reconciled with proper hand-crafted priors help boost the performance of deblurring.

4.2.2 The Influence of Different Architectures for DRP

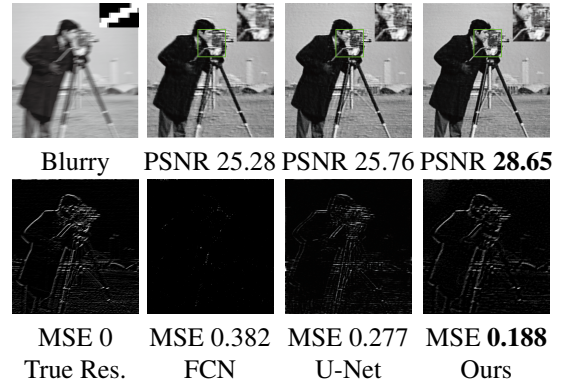


Figure 6. The influence of different network architectures for DRP. The deblurred results (row 1) and estimated residuals (row 2) from *Cameraman* blurred by a motion kernel with a length of 20 pixels and an orientation of 10° . The input inaccurate blur kernel for deblurring has a length of 20 pixels and an orientation of 20° .

In this experiment, we compare the results returned by three network architectures for modeling the residual: (i) FCN, (ii) U-Net, and (iii) the proposed customized U-Net (see Figure 5). We can observe from the results in Figure 6 that FCN is almost impotent to characterize any components in the residual while U-Net weakly captures the rough

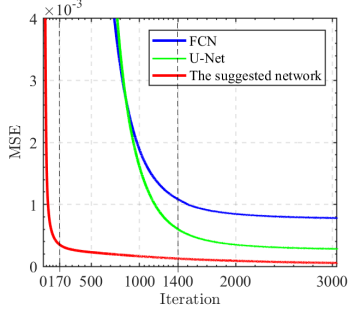


Figure 7. The MSE values on the residual r estimated by different network architectures with respect to the iteration number.

frame. In comparison, the customized U-Net is capable of seizing the fine structure of the residual.

Figure 7 displays the MSE values on the residual r estimated by different networks with respect to the iteration number. This indicates that the customized U-Net leads to a faster convergence and better result. When the number of iterations reaches 170, the curve of the customized U-Net starts to gradually stabilize while after about 1,400 iterations, a similar behavior occurs in the optimization process with U-Net and FCN. In this example, the running time consumed to reach the minimizer is 51 (sec.) for the customized U-Net, 380 for U-Net, and 405 for FCN, respectively.

4.3. Performance on Benchmark Datasets

We compare the proposed method with state-of-the-art deblurring methods on simulated and real data. We evaluate the performance of the proposed method over the benchmark datasets of Levin *et al.* and Lai *et al.* [11, 12]. Levin *et al.* [12] contains 32 blurred samples corresponding to 4 sharp images convolved with 8 blur kernels. Lai *et al.* [11] contains both real and simulated images, which are blurry with 25 sharp images and 4 blur kernels. The Gaussian noise level is set to be 1%.

Kernel Estimation. The input inaccurate kernels for Levin *et al.* dataset are obtained by applying five blind deblurring algorithms on the blurry images, including Cho *et al.* [1], SelfDeblur by Ren *et al.* [19], Levin *et al.* [12], Pan *et al.* [17], and Sun *et al.* [25]. The estimated kernels for Lai *et al.* [11] are obtained by blind deblurring methods including Xu *et al.* [30], Xu *et al.* [14], Sun *et al.* [25], and Perrone *et al.* [2].

Compared Methods. We select seven state-of-the-art methods as the baselines. These methods cover a double-DIP based blind deblurring (BD) method SelfDeblur [19], three non-blind (NBD) deblurring methods [18, 23, 33] and three semi-blind deblurring (SBD) methods [4, 6, 28, 34]. Note that, to model the kernel error, Zhao *et al.*, Ji & Wang [6, 34] use hand-crafted priors while Vasu *et al.* and Fang *et al.* [4, 28] use data-driven prior.

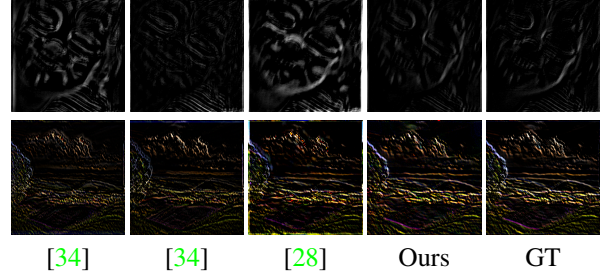


Figure 8. The estimated residual from semi-blind methods on the datasets of Levin *et al.* [12] and Lai *et al.* [11].

Tables 2 and 3 show the average PSNR/SSIM of different methods on datasets Levin *et al.* and Lai *et al.*. In terms of the average PSNR and SSIM, we observe that the proposed method performs competitively against the compared methods. The double DIP-based SelfDeblur without handling kernel uncertainty which simply imposes DIP on the latent image does not show competitive performance. Generally, data-driven prior based methods [28, 33] show better performance than hand-crafted prior based methods. Due to the diversity of blurs and images, the data-driven prior based method [28] performs even worse than hand-crafted prior methods in some cases. In comparison, the proposed method outperforms both hand-crafted prior based and data-driven prior based methods.

Figure 8 and Figure 9 illustrate visual results obtained by different methods. From Figure 8, we observe that our method can capture the fine details of residuals. And from Figure 9, we observe that our method recovers the latent images better than the competing methods. Notably, methods without handling the kernel uncertainty show severe ringing artifacts in the restored images while the proposed method suppresses them well as illustrated in row 2 of Figure 9.

These results verify the effectiveness of the proposed method, driven by the fine representation ability of DRP of capturing the residual induced by the kernel error. The visual quality of the proposed method is also consistent with the improvement of quantitative performance gain.

Then we compare our method with the baselines of NBD and SBD methods on real-world images from dataset Lai *et al.* [11]. The kernels are estimated by [17]. From Figure 10, we can see that NBD methods [18, 23] yield significant ringing artifacts in restored images. Among the SBD methods, hand-crafted prior based methods [6, 34] perform unpleasantly in deblurring while the data-driven prior based method [28] slightly arouse outliers and artifacts. In comparison, our method shows good restored image quality and robustness to ringing artifacts.

Table 2. Average PSNR/SSIM comparison of all the tested methods on the dataset of Levin *et al.* [12] with $\sigma = 1\%$ using different kernels estimated by 5 methods.

Method Kernel	BD	NBD			SBD				
	[19]	[10]	[18]	[33]	[34]	[6]	[28]	[4]	Ours
[1]	28.52/0.80	28.12/0.82	28.49/0.81	28.57/0.82	28.76/0.82	28.55/0.83	29.50/0.84	29.86/0.85	30.52/0.88
[13]		28.17/0.83	28.55/0.83	28.98/0.84	27.96/0.81	28.79/0.83	29.65/0.85	29.91/0.86	30.78/0.89
[19]		27.88/0.82	27.59/0.80	27.68/0.82	27.19/0.80	27.39/0.82	29.01/0.85	28.57/0.83	29.55/0.86
[17]		29.84/0.86	29.99/0.86	30.57/0.87	28.98/0.83	29.21/0.86	31.62/0.87	31.98/0.91	32.28/0.92
[25]		29.30/0.85	29.91/0.86	30.89/0.87	28.99/0.83	29.10/0.86	30.75/0.88	31.05/0.89	31.84/0.91

Table 3. Average PSNR/SSIM comparison of all the tested methods on the dataset of Lai *et al.* [11] with $\sigma = 1\%$ using different kernels estimated by 4 methods.

Method Kernel	BD	NBD			SBD				
	[19]	[10]	[18]	[33]	[34]	[6]	[28]	[4]	Ours
[30]	17.69/0.64	17.73/0.65	17.61/0.56	17.88/0.60	19.60/0.64	19.67/0.61	20.21/0.67	20.67/0.65	21.07/0.68
[14]		18.83/0.62	17.81/0.57	17.99/0.62	19.78/0.67	19.34/0.60	19.52/0.64	20.25/0.62	20.96/0.68
[25]		17.96/0.61	17.99/0.57	18.12/0.64	19.83/0.69	20.09/0.68	19.88/0.67	20.44/0.66	21.03/0.70
[2]		17.57/0.63	16.88/0.54	17.53/0.62	19.56/0.65	19.21/0.60	19.12/0.60	19.87/0.60	20.31/0.64

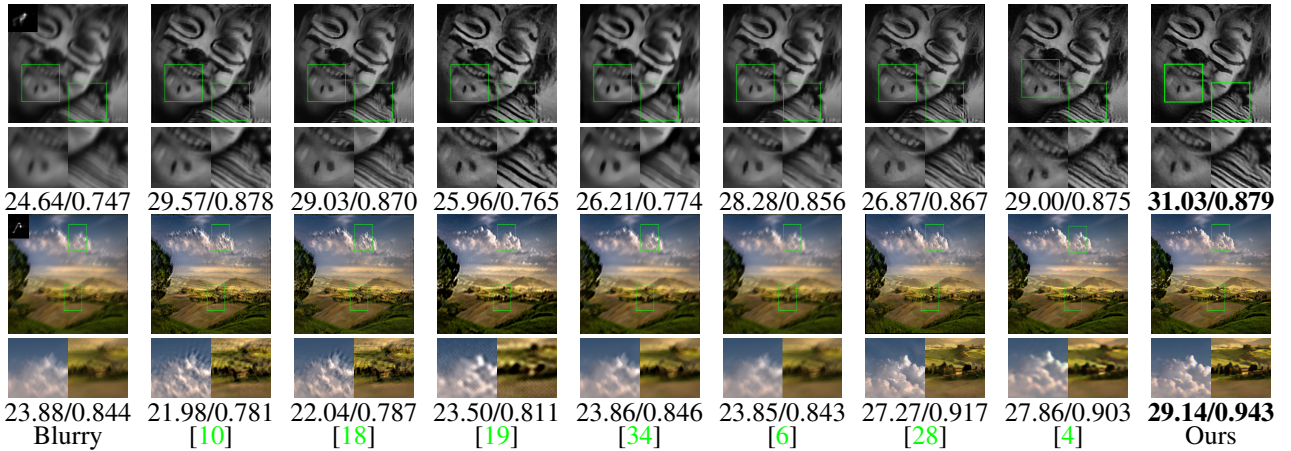


Figure 9. The deblurred results by different methods on the datasets of Levin *et al.* [12] with the kernel estimated by [1] and Lai *et al.* [11] with the kernel estimated by [2]. The numerical indexes at the bottom of each image indicate the PSNR and SSIM values.

4.4. Performance on Multiple Blur Scenarios

In this part, we explore the robustness to the kernel error and the adaptability to different blurs of the proposed method. Three typical blur kernels, including Motion, Gaussian, and Disk are employed.

Inaccurate Kernel Setup. The true kernels are a motion blur kernel with 20 pixels length and 10° orientation, denoted by Motion (20, 10); a Gaussian blur with size 20×20 and $\sigma = 4$, denoted by Gaussian (20, 4); and a disk-like defocus blur with a radius of 4 pixels, denoted by Disk (4). The inaccurate kernel inputs are generated by varying parameters of the blur kernel.

Compared Methods. Five methods are selected as comparisons, including NBD [6, 10, 18] and SBD [16, 28] meth-

ods. In particular, the data-driven prior based method [16] unrolled an iterative total-least-squares estimator in which the residual priors are learned by their customized supervised Dual-path U-Net.

Figure 11 displays the PSNR values against the bias of inaccurate kernels. Obviously, when the blur kernel is inaccurate, hand-crafted prior based methods [6, 10, 18] generally are inferior to data-driven prior based methods [16, 28]. Due to the nature of supervision learning, they perform well in the case of motion blur, but fail to continue their impressive performances in the case of Gaussian and Disk blur. In comparison, our method achieves the best performance while showing great adaptability to three kinds of blurs.

On the other hand, the PSNR values of deblurred results by NBD methods significantly go down as the bias



Figure 10. The deblurred results by different methods on the real images from the dataset of Lai *et al.* [11].

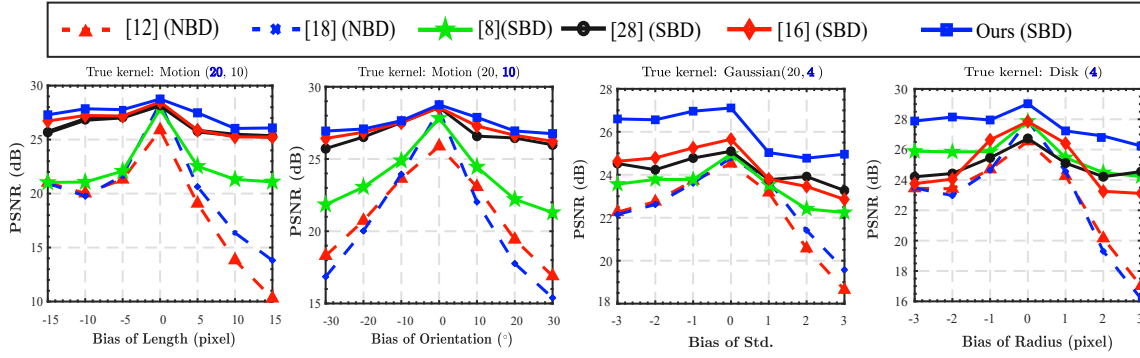


Figure 11. PSNR values against bias of inaccurate kernel parameters obtained by different methods.

increases, which implies the importance of handling kernel uncertainty. When the bias expands, the PSNR value of the proposed method tends to decline more slightly than other SBD methods, outperforming all the competing methods. This result supports that our method shows greater robustness to the kernel error than the baseline methods.

5. Conclusion

We proposed a data-free deep prior (DRP) for the residual induced by the kernel error expressed by a customized untrained deep neural network, which allows us to flexibly adapt to different blurs and images in real scenarios. By organically integrating the respective strengths of deep priors and hand-crafted priors, we proposed an unsupervised semi-blind deblurring model which recovers the latent image from the blurry image and inaccurate blur kernel. To tackle the formulated model, we developed an alternating minimization algorithm. Extensive experiments on multiple cases showed that the proposed method achieves notable

performance compared with the state-of-the-art methods in terms of image quality and robustness to the kernel error.

References

- [1] Sunghyun Cho and Seungyong Lee. Fast motion deblurring. In *ACM SIGGRAPH Asia 2009 papers*, pages 1–8. 2009. 6, 7
- [2] Perrone Daniele and Favaro Paolo. Total variation blind deconvolution: The devil is in the details. In *CVPR*, pages 2909–2916, 2014. 6, 7
- [3] Weisheng Dong, Lei Zhang, Guangming Shi, and Xin Li. Nonlocally centralized sparse representation for image restoration. *IEEE TIP*, 22(4):1620–1630, 2013. 2
- [4] Yingying Fang, Hao Zhang, Hok Shing Wong, and Tiejiong Zeng. A robust non-blind deblurring method using deep denoiser prior. In *CVPRW*, pages 735–744, June 2022. 6, 7, 8
- [5] Yosef Gandelsman, Assaf Shocher, and Michal Irani. "double-dip": Unsupervised image decomposition via coupled deep-image-priors. In *CVPR*, pages 11026–11035,

2019. 3
- [6] Hui Ji and Kang Wang. Robust image deblurring with an inaccurate blur kernel. *IEEE TIP*, 21(4):1624–1634, 2011. 1, 2, 3, 6, 7, 8
 - [7] Jiaya Jia. Single image motion deblurring using transparency. In *CVPR*, pages 1–8, 2007. 1
 - [8] Liu Jun, Yan Ming, and Zeng Tiejong. Surface-aware blind image deblurring. *IEEE TPAMI*, 43(3):1041–1055, 2021. 1
 - [9] Diederick P Kingma and Jimmy Ba. Adam: A method for stochastic optimization. In *ICLR*, 2015. 4
 - [10] Dilip Krishnan and Rob Fergus. Fast image deconvolution using hyper-laplacian priors. *NIPS*, 22, 2009. 2, 7, 8
 - [11] Wei-Sheng Lai, Jia-Bin Huang, Zhe Hu, Narendra Ahuja, and Ming-Hsuan Yang. A comparative study for single image blind deblurring. In *CVPR*, pages 1701–1709, 2016. 6, 7, 8
 - [12] Anat Levin, Yair Weiss, Fredo Durand, and William T Freeman. Understanding and evaluating blind deconvolution algorithms. In *CVPR*, pages 1964–1971, 2009. 1, 6, 7
 - [13] Anat Levin, Yair Weiss, Fredo Durand, and William T Freeman. Efficient marginal likelihood optimization in blind deconvolution. In *CVPR*, pages 2657–2664, 2011. 7
 - [14] Xu Li, Zheng Shicheng, and Jia Jiaya. Unnatural l0 sparse representation for natural image deblurring. In *CVPR*, pages 1107–1114, 2013. 6, 7
 - [15] Guangcan Liu, Shiyu Chang, and Yi Ma. Blind image deblurring using spectral properties of convolution operators. *IEEE TIP*, 23(12):5047–5056, 2014. 1
 - [16] Yuesong Nan and Hui Ji. Deep learning for handling kernel/model uncertainty in image deconvolution. In *CVPR*, pages 2388–2397, 2020. 2, 7
 - [17] Jinshan Pan, Deqing Sun, Hanspeter Pfister, and Ming-Hsuan Yang. Blind image deblurring using dark channel prior. In *CVPR*, pages 1628–1636, 2016. 1, 6, 7
 - [18] Dongwei Ren, Hongzhi Zhang, David Zhang, and Wangmeng Zuo. Fast total-variation based image restoration based on derivative alternated direction optimization methods. *Neurocomputing*, 170:201–212, 2015. 6, 7, 8
 - [19] Dongwei Ren, Kai Zhang, Qilong Wang, Qinghua Hu, and Wangmeng Zuo. Neural blind deconvolution using deep priors. In *CVPR*, pages 3341–3350, 2020. 3, 6, 7
 - [20] Dongwei Ren, Wangmeng Zuo, David Zhang, Jun Xu, and Lei Zhang. Partial deconvolution with inaccurate blur kernel. *IEEE TIP*, 27(1):511–524, 2017. 2
 - [21] Dongwei Ren, Wangmeng Zuo, David Zhang, Lei Zhang, and Ming-Hsuan Yang. Simultaneous fidelity and regularization learning for image restoration. *IEEE TPAMI*, 43(1):284–299, 2019. 2
 - [22] Wenqi Ren, Xiaochun Cao, Jinshan Pan, Xiaojie Guo, Wangmeng Zuo, and Ming-Hsuan Yang. Image deblurring via enhanced low-rank prior. *IEEE TIP*, 25(7):3426–3437, 2016. 1
 - [23] Fergus Rob, Singh Barun, Hertzmann Aaron, Roweis Sam T, and Freeman William T. Removing camera shake from a single photograph. In *ACM SIGGRAPH 2006 Papers*, pages 787–794, 2006. 1, 6
 - [24] Raúl Rojas. *The Backpropagation Algorithm*, pages 149–182. Springer Berlin Heidelberg, Berlin, Heidelberg, 1996. 4
 - [25] Libin Sun, Sunghyun Cho, Jue Wang, and James Hays. Edge-based blur kernel estimation using patch priors. In *IEEE International Conference on Computational Photography*, pages 1–8, 2013. 1, 6, 7
 - [26] Michaeli Tomer and Irani Michal. Blind deblurring using internal patch recurrence. In *ECCV*, pages 783–798, 2014. 1
 - [27] Dmitry Ulyanov, Andrea Vedaldi, and Victor Lempitsky. Deep image prior. In *CVPR*, pages 9446–9454, 2018. 3
 - [28] Subeesh Vasu, Venkatesh Reddy Maligireddy, and AN Rajagopalan. Non-blind deblurring: Handling kernel uncertainty with cnns. In *CVPR*, pages 3272–3281, 2018. 1, 2, 6, 7, 8
 - [29] Yilun Wang, Junfeng Yang, Wotao Yin, and Yin Zhang. A new alternating minimization algorithm for total variation image reconstruction. *SIAM Journal on Imaging Sciences*, 1(3):248–272, 2008. 2
 - [30] Li Xu and Jiaya Jia. Two-phase kernel estimation for robust motion deblurring. In *ECCV*, pages 157–170, 2010. 6, 7
 - [31] Yanyang Yan, Wenqi Ren, Yuanfang Guo, Rui Wang, and Xiaochun Cao. Image deblurring via extreme channels prior. In *CVPR*, pages 4003–4011, 2017. 1
 - [32] Jiawei Zhang, Jinshan Pan, Wei-Sheng Lai, Rynson WH Lau, and Ming-Hsuan Yang. Learning fully convolutional networks for iterative non-blind deconvolution. In *CVPR*, pages 3817–3825, 2017. 2
 - [33] Kai Zhang, Wangmeng Zuo, Shuhang Gu, and Lei Zhang. Learning deep cnn denoiser prior for image restoration. In *CVPR*, pages 3929–3938, 2017. 2, 6, 7
 - [34] Xile Zhao, Wei Wang, Tiejong Zeng, Tingzhu Huang, and Michael K. Ng. Total variation structured total least squares method for image restoration. *SIAM Journal on Imaging Sciences*, 35, 2013. 2, 6, 7, 8
 - [35] Changyin Zhou, Stephen Lin, and Shree K Nayar. Coded aperture pairs for depth from defocus and defocus deblurring. *IJCV*, 93(1):53–72, 2011. 1
 - [36] Wangmeng Zuo, Dongwei Ren, David Zhang, Shuhang Gu, and Lei Zhang. Learning iteration-wise generalized shrinkage-thresholding operators for blind deconvolution. *IEEE TIP*, 25(4):1751–1764, 2016. 1